Euro. Jnl of Applied Mathematics (2008), *vol.* 19, *pp.* 541–560.
doi:10.1017/S0956792508007596 Printed in the United Kingdom

Singular perturbation analysis of the steady-state Poisson–Nernst–Planck system: Applications to ion channels

A. SINGER[1], D. GILLESPIE[2], J. NORBURY[3] and R. S. EISENBERG[2]

[1]*Program in Applied Mathematics, Department of Mathematics, Yale University, 10 Hillhouse Ave., PO Box 208283, New Haven, CT 06520-8283, USA*
[2]*Department of Molecular Biophysics and Physiology, Rush Medical Center, 1750 West Harrison Street, Chicago, IL 60612, USA*
[3]*OCIAM, Mathematical Institute, Oxford University, 27–29 St Giles', Oxford OX1 3LB, UK*

(*Received 23 January 2007; revised 28 April 2008; first published online 6 June 2008*)

Ion channels are proteins with a narrow hole down their middle that control a wide range of biological function by controlling the flow of spherical ions from one macroscopic region to another. Ion channels do not change their conformation on the biological time scale once they are open, so they can be described by a combination of Poisson and drift-diffusion (Nernst–Planck) equations called PNP in biophysics. We use singular perturbation techniques to analyse the steady-state PNP system for a channel with a general geometry and a piecewise constant permanent charge profile. We construct an outer solution for the case of a constant permanent charge density in three dimensions that is also a valid solution of the one-dimensional system. The asymptotical current–voltage (I–V) characteristic curve of the device (obtained by the singular perturbation analysis) is shown to be a very good approximation of the numerical I–V curve (obtained by solving the system numerically). The physical constraint of non-negative concentrations implies a unique solution, i.e., for each given applied potential there corresponds a unique electric current (relaxing this constraint yields non-physical multiple solutions for sufficiently large voltages).

1 Introduction

The prediction of ionic currents through protein channels as a function of the ionic concentration, the applied voltage and the structure of the channel is one of the fundamental problems in molecular biophysics [15]. On the one hand, the function of the channel depends on its microscopic geometry and content (i.e., permanent charges) which are in the atomic level and are characterized by atomic length scales – the diameter of the channel is just a few angstroms. On the other hand, the ionic currents going through the channel are driven by macroscopic conditions. The currents are due to the applied electric potential and different ionic bath concentrations. These conditions are prescribed at a macroscopic distance away from the channel. The concentration and electric potential are unknown at the two ends of the channel. In other words, the ion channel is an atomic device. The multi-scale challenge is to understand the function of an atomic device from the prescribed macroscopic conditions.

Different channels have different geometries which can be quite complicated. Crudely speaking, the channel itself may be viewed as a pipe (cylinder) embedded in an impermeable membrane. The access region to the channel is roughly a funnel, for example, a cone. The transition geometry between the channel and the access region is smooth. It is expected that the function of the channel will depend on both its geometrical properties such as the diameter and length of the cylinder and also the geometrical properties of the access region such as the opening angle of the cone. Furthermore, nowadays, it is also possible to artificially build plastic nano-channels of roughly similar geometries and similar (although distinct) function [25, 26].

The Poisson-Nernst-Planck (PNP) equations have been proposed as the basic continuum model for ion channels [10]. PNP is also known as the drift-diffusion equations in the semiconductor literature [20], the crucial point (in both channels and semiconductors) being that the electric field is calculated from all the charges present. The electric field is not set independently of the rest of the model as it is in traditional channel models [15]. The continuum PNP system was derived from a microscopic model of Langevin trajectories in the limit of large damping and neglecting correlations of different ionic trajectories [23]. It also neglects finite size effects due to the finite size of ions. Finite size effects are approximately captured, as they are in equilibrium models of bulk solutions [2, 5, 7, 8, 9, 12, 24], by adding a suitable 'excess' term to the chemical potential [14, 21].

The dimensionless version of the time-dependent PNP equations for a system of two ionic species with opposite charges is given by

$$\frac{\lambda^2}{a^2}\Delta\phi = n - p - q, \tag{1.1}$$

$$\boldsymbol{J}^n = D_n\left(-\nabla n + n\nabla\phi\right), \tag{1.2}$$

$$\boldsymbol{J}^p = D_p\left(-\nabla p - p\nabla\phi\right), \tag{1.3}$$

$$-\nabla\cdot\boldsymbol{J}^n = \nabla\cdot\left[D_n\left(\nabla n - n\nabla\phi\right)\right] = \frac{\partial n}{\partial t}, \tag{1.4}$$

$$-\nabla\cdot\boldsymbol{J}^p = \nabla\cdot\left[D_p\left(\nabla p + p\nabla\phi\right)\right] = \frac{\partial p}{\partial t}, \tag{1.5}$$

where ϕ is the electric potential, n is the density of the negative charged ions, p is the density of the positive charged ions, q is the permanent charge of the channel, $\boldsymbol{J}^n$, $\boldsymbol{J}^p$ are the ionic flux densities and D_n, D_p are their diffusion coefficients. The Debye length λ is scaled with the maximum of q and is typically a few angströms or smaller long. We scale spatial coordinates with a, where a^2 is the cross-section area of the channel. This implies that all flux densities are scaled with $1/a$, whereas total fluxes are scaled with a. The steady-state PNP equations are obtained by setting the time derivatives $\partial n/\partial t, \partial p/\partial t$ to 0. The only non-dimensional parameter in the problem is $\varepsilon = \lambda/a$.

Boundary conditions for the PNP system (1.1)–(1.5) must be prescribed as well, because they drive the system out of equilibrium and produce the non-vanishing ionic fluxes. The boundary conditions are given by (see Figure 1)

$$\frac{\partial\phi}{\partial v} = \frac{\partial n}{\partial v} = \frac{\partial p}{\partial v} = 0, \qquad \text{for } \boldsymbol{x}\in\partial\Omega_{\mathrm{r}}, \tag{1.6}$$

$$\phi \to \phi_L, \quad \text{for } z\to-\infty, \tag{1.7}$$

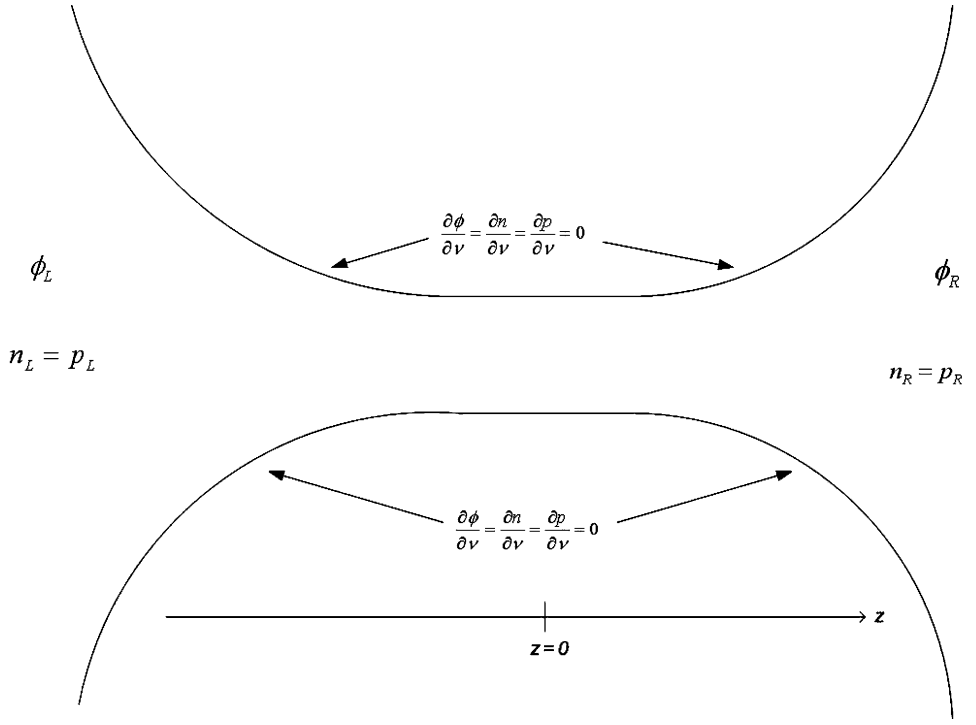

FIGURE 1. The ion channel geometry and boundary conditions: z measures distance symmetrically through the channel from the left bath to the right bath. The membrane walls are both flux-free and electrically insulating to leading order.

$$\phi \to \phi_R, \qquad \text{for } z \to +\infty, \tag{1.8}$$

$$n, p \to n_L = p_L, \quad \text{for } z \to -\infty, \tag{1.9}$$

$$n, p \to n_R = p_R, \quad \text{for } z \to +\infty. \tag{1.10}$$

where $\partial\Omega_r$ is the reflecting part of the boundary, i.e., the biological membrane, and ν is the unit normal of the boundary. The reflecting boundary condition (1.6) $\frac{\partial \phi}{\partial \nu} = 0$ approximates the 'jump condition' of the electric field due to the significant difference between the dielectric constants in water and membrane. Furthermore, a reflecting boundary condition usually means the no-flux condition, e.g., $\boldsymbol{J}^n \cdot \nu = \boldsymbol{J}^p \cdot \nu = 0$. At the boundary $\frac{\partial \phi}{\partial \nu} = 0$, and equations (1.2)–(1.3) show that the no-flux boundary condition is equivalent to (1.6).

The recent mathematical analysis of the PNP system applied to channels [1, 11, 16] focuses on a one-dimensional version of the PNP system

$$\varepsilon^2 \frac{d^2\phi}{dz^2} = n - p - q, \tag{1.11}$$

$$\frac{dn}{dz} - n\frac{d\phi}{dz} = -J^n/D_n, \tag{1.12}$$

$$\frac{dp}{dz} + p\frac{d\phi}{dz} = -J^p/D_p, \tag{1.13}$$

with boundary conditions prescribed at the two ends of the channel: J^n, J^p are the total fluxes which are unknown and $\varepsilon \ll 1$. However, the one-dimensional model incorporates some conceptual failures. The boundary conditions in the one-dimensional model (1.11)–(1.13) are prescribed at the two ends of the channel. Notwithstanding, the actual values of the potential and concentrations are unknown there and are only known at a macroscopic distance away from the channel. Furthermore, as stated above, the one-dimensional model cannot capture any geometrical effects.

Nonner and Eisenberg [22] suggested the following one-dimensional approximation of the three-dimensional PNP system (aka the slowly varying approximation; see also [13, chapter 2, pp. 14–24]):

$$\frac{\varepsilon^2}{A(z)}\frac{d}{dz}\left(A(z)\frac{d\phi}{dz}\right) = n - p - q, \tag{1.14}$$

$$A(z)\left[\frac{dn}{dz} - n\frac{d\phi}{dz}\right] = -J^n/D_n, \tag{1.15}$$

$$A(z)\left[\frac{dp}{dz} + p\frac{d\phi}{dz}\right] = -J^p/D_p, \tag{1.16}$$

where J^n and J^p are once again the total fluxes. The function $A(z)$ represents the surface area of equipotential shells. The area function $A(z)$ grows indefinitely with z into the bath, such as the explicit example of [6] which we consider later:

$$A(z) = 1 + z^2, \quad -\infty < z < \infty. \tag{1.17}$$

The fundamental drift-diffusion device equations of semiconductors are similar to the PNP system, and it is therefore not surprising that the classical singular perturbation analysis of semiconductors [17–20] is applicable for ion channels as well. Yet, there are major differences between ion channels and semiconductors, even in the simplest modelling level, that call for important modifications. The parameter ε for semiconductors ($\sim 10^{-5}$) is much smaller than in ion channels. The geometry of an ion channel is much different than that of a semiconductor device. The microscopic size of the channel makes the effective ε to be much larger. In some cases, the two junction layers overlap without an outer zone [14], which means that ε is not a small parameter. Another difference between the two is expressed through the ratio of the doping charge density to the carrier charge density of the bath (rather than in the 'doped' region, where electro-neutrality renders the ratio to be almost one). In semiconductors this ratio can be as large as 10^4–10^5 [18] in favour of the doping charge density, whereas for channels the ratio is typically much smaller and can be of the order of one.

Mathematically, in semiconductors the exact outer solutions are not of great importance, and the solution is mostly determined by the boundary layer solution in the junction region, whereas for channels, the outer solutions and boundary layers are both significant. Finally, in the channel problem there can be more than two ionic species with different valencies (e.g., $+1$, $+2$, -1) which leads to rich behaviour. For example, channels can suck up micromolar calcium, where the aforementioned ratio of permanent charge to carrier density is of order one for sodium, but 10^6 for calcium. In a finer level of modelling, it

is well known that certain aspects of the behaviour of channels, such as selectivity, are often explained by finite size effects [14, 21] that do not play a role in semiconductors.

Barcilon *et al.* [1] analysed (1.11)–(1.13) on a finite interval without permanent charge ($q = 0$) as a classical singular perturbation problem. Liu [11, 16] recently analysed a similar problem using the geometric singular perturbation approach. Gillespie [13] used singular perturbation analysis to explore many other cases, including a general geometry function $A(z)$, a piecewise constant permanent charge profile q and space-dependent diffusion coefficients (MD simulations suggest that the diffusion coefficient in a microscopic channel is much smaller than in the bulk [27, 29]) that are possibly different for the different ionic species.

In this paper we use singular perturbation techniques to analyse the steady-state PNP system for a channel with a general geometry and a piecewise constant permanent charge profile. Using a suitable transformation, we convert the one-dimensional system (1.14)–(1.16) to (1.11)–(1.13) with an additional geometry factor appearing only in the Poisson equation. We construct an outer solution for the case of a constant permanent charge density in three dimensions that also holds as the solution of the one-dimensional system. Matching the boundary layer solution and the outer solution at the junction (the discontinuity point of the permanent charge) is possible without solving the boundary layer (Poisson–Boltzmann) equations explicitly. We focus on the case of two ionic species in a charged channel and later on the specific geometry (1.17). The asymptotical current–voltage (I–V) characteristic curve of the device (obtained by the singular perturbation analysis) is shown to be a very good approximation of the numerical I–V curve (obtained by solving the system (1.14)–(1.16) numerically). The physical constraint of non-negative concentrations implies a unique solution, i.e., for each given applied potential there corresponds a unique electric current (relaxing this constraint yields non-physical multiple solutions for sufficiently large voltages). Some results in this paper have appeared in a doctoral thesis [13] and the Study Group Report [6]; we are pleased to report them here. The case of three ionic species with different valencies and different diffusion coefficients will be considered in a future paper.

2 Outer solution with constant permanent charge density in three dimensions

Consider the three-dimensional steady-state PNP system (1.1)–(1.5) after the linear transformation to net charge $Q = n - p$ and total concentration $C = n + p$ variables to be given by

$$\varepsilon^2 \Delta\phi = Q - q, \tag{2.1}$$

$$\nabla \cdot [\nabla Q - C\nabla\phi] = 0, \tag{2.2}$$

$$\nabla \cdot [\nabla C - Q\nabla\phi] = 0. \tag{2.3}$$

In this first paper, we assume for algebraic simplicity equal diffusion coefficients $D_n = D_p = 1$. The permanent charge density q is assumed to be piecewise constant, that is, it has constant value q_0 inside a narrow region (i.e., the channel) and vanishes elsewhere (in the two baths). All functions satisfy no-flux (homogeneous Neumann) boundary conditions on the surface of the membrane, and Dirichlet boundary (aka far field) conditions at the

left and right infinities with prescribed concentration values $C \to C_L, C_R$, potential values $\phi \to \phi_L, \phi_R$ and electro-neutrality $Q \to 0$ (see equations (1.6)–(1.10)).

We look for an outer solution of the form

$$\phi^{OUT} = \phi_0^{OUT} + \varepsilon\phi_1^{OUT} + \cdots, \tag{2.4}$$

$$Q^{OUT} = Q_0^{OUT} + \varepsilon Q_1^{OUT} + \cdots, \tag{2.5}$$

$$C^{OUT} = C_0^{OUT} + \varepsilon C_1^{OUT} + \cdots. \tag{2.6}$$

Odd powers of ε are included in the expansion, because we expect the formation of boundary layers (inner solutions) at the junctions, where q is discontinuous. In this paper we calculate the leading order terms.

The leading order equations are

$$Q_0^{OUT} = q, \tag{2.7}$$

$$\nabla \cdot \left[\nabla Q_0^{OUT} - C_0^{OUT}\nabla\phi_0^{OUT}\right] = 0, \tag{2.8}$$

$$\nabla \cdot \left[\nabla C_0^{OUT} - Q_0^{OUT}\nabla\phi_0^{OUT}\right] = 0. \tag{2.9}$$

Electro-neutrality is expressed in (2.7). Next, we show that (2.8)–(2.9) imply the relation[1]

$$\phi_0^{OUT} = \alpha \ln\left(C_0^{OUT} + \alpha q\right) + \beta, \tag{2.10}$$

where α and β are constants, to be later determined by matching and boundary conditions. Indeed, $Q_0^{OUT} \equiv \text{const}$, therefore $\nabla Q_0^{OUT} = 0$, and equation (2.8) reads

$$\nabla \cdot \left(C_0^{OUT}\nabla\phi_0^{OUT}\right) = 0. \tag{2.11}$$

We verify that relation (2.10), which can also be written in the differential form

$$\nabla\phi_0^{OUT} = \frac{\alpha}{C_0^{OUT} + \alpha q}\nabla C_0^{OUT} \tag{2.12}$$

satisfies (2.9). Indeed,

$$\begin{aligned}
\nabla \cdot \left(\nabla C_0^{OUT} - Q_0^{OUT}\nabla\phi_0^{OUT}\right) &= \nabla \cdot \left(\nabla C_0^{OUT} - q\nabla\phi_0^{OUT}\right) \\
&= \nabla \cdot \left(\nabla C_0^{OUT} - q\frac{\alpha}{C_0^{OUT} + \alpha q}\nabla C_0^{OUT}\right) \\
&= \nabla \cdot \left(\frac{C_0^{OUT}}{C_0^{OUT} + \alpha q}\nabla C_0^{OUT}\right) \\
&= \frac{1}{\alpha}\nabla \cdot \left(C_0^{OUT}\nabla\phi_0^{OUT}\right) = 0,
\end{aligned} \tag{2.13}$$

by (2.11). Equation (2.12) indicates that the homogeneous Neumann boundary conditions are satisfied by C_0^{OUT} and ϕ_0^{OUT} if any linear combination of them satisfies this boundary condition.

[1] The relation (2.10) for the particular case $q = 0$ was introduced in the Study Group meeting by Professor John King [6, p. 6, eq. (3.16)]. A similar relation for the one-dimensional case appears in [13, p. 59, eq. (4.53)] and [1, p. 637, eqs. (45)–(47)].

The calculation (2.13) also shows that the constant α is the proportionality constant between the electric current $\boldsymbol{J}^e = \boldsymbol{J}^n - \boldsymbol{J}^p$ and the diffusion current $\boldsymbol{J}^d = \boldsymbol{J}^n + \boldsymbol{J}^p$

$$\boldsymbol{J}_0^e = -\left[\nabla Q_0^{\mathrm{OUT}} - C_0^{\mathrm{OUT}} \nabla \phi_0^{\mathrm{OUT}}\right] = \alpha\left[\nabla C_0^{\mathrm{OUT}} - Q_0^{\mathrm{OUT}} \nabla \phi_0^{\mathrm{OUT}}\right] = -\alpha \boldsymbol{J}_0^d. \tag{2.14}$$

Note that $Q_0^{\mathrm{OUT}} \equiv \text{const}$, consequently (2.9) gives in the outer zone

$$\Delta\left(C_0^{\mathrm{OUT}} - q\phi_0^{\mathrm{OUT}}\right) = 0, \tag{2.15}$$

that is, $C_0^{\mathrm{OUT}} - q\phi_0^{\mathrm{OUT}}$ is a harmonic function, for which Neumann boundary conditions are prescribed (note that $q\phi_0^{\mathrm{OUT}}$ is physically interpreted as the energy of the capacitor, or the energy to put the doping charge q where it is with potential ϕ_0^{OUT} – this is the minimal electrostatic work needed to build the protein from a hypothetic uncharged precursor). Combining equations (2.10) and (2.15) we conclude that

$$\left(C_0^{\mathrm{OUT}} + \alpha q\right) - \alpha q \ln\left(C_0^{\mathrm{OUT}} + \alpha q\right) \tag{2.16}$$

is a harmonic function.

2.1 The case $q \equiv 0$, Ohm's law and Fick's law

In the special case where there is no permanent charge, i.e., $q \equiv 0$, it is possible to find explicit current–voltage relations.

Substituting $q = 0$ in relations (2.10) and (2.15) gives

$$\phi_0^{\mathrm{OUT}} = \alpha \ln C_0^{\mathrm{OUT}} + \beta, \tag{2.17}$$

where C_0^{OUT} is a harmonic function ($\Delta C_0^{\mathrm{OUT}} = 0$). The constants α and β are determined by the boundary conditions

$$\phi_0^{\mathrm{OUT}} = \phi_{\mathrm{L}} + \frac{\phi_{\mathrm{L}} - \phi_{\mathrm{R}}}{\ln C_{\mathrm{L}} - \ln C_{\mathrm{R}}}\left(\ln C_0^{\mathrm{OUT}} - \ln C_{\mathrm{L}}\right). \tag{2.18}$$

The absence of permanent charge simplifies the relation for the leading order electric current and diffusion current (2.14)

$$\boldsymbol{J}_0^d = \nabla C_0^{\mathrm{OUT}}, \tag{2.19}$$

$$\boldsymbol{J}_0^e = \frac{\phi_{\mathrm{L}} - \phi_{\mathrm{R}}}{\ln C_{\mathrm{L}} - \ln C_{\mathrm{R}}} \nabla C_0^{\mathrm{OUT}}. \tag{2.20}$$

Fick's law is depicted in equation (2.19) stating the diffusion flux equals the gradient of the concentration. Ohm's law is rendered in equation (2.20) showing the electric current is proportional to the applied voltage $\phi_{\mathrm{L}} - \phi_{\mathrm{R}}$.

The total fluxes (integrated over any cross section) depend on the specific structure, because the harmonic function determining the concentration profile is geometry-dependent. We consider the example given in [6, p. 7] chosen for its mathematical simplicity as it allows a separation of variables solution. We find equivalent formulas for our variables

to those given in [6, p. 8]. The example is that of a channel lying inside the hyperboloid

$$\frac{\rho^2}{\cos^2\Theta} - \frac{z^2}{\sin^2\Theta} = 1, \tag{2.21}$$

where ρ and z are cylindrical polar coordinates and Θ parameterize the hyperboloid. Note that $\Theta = 0$ corresponds to an impermeable boundary at $z = 0$, $\rho > 1$ and a hole at $z = 0, \rho < 1$. Note also that the hyperboloid gives a good approximation to the funnel shape of the protein associated with the ion channel. Introducing oblate spheroidal coordinates

$$\rho = \cosh\xi\cos\eta, \quad z = \sinh\xi\sin\eta, \tag{2.22}$$

the domain lies in $-\infty < \xi < \infty$, $\Theta < \eta \leqslant \pi/2$. Separation of variables gives the concentration

$$C_0^{\mathrm{OUT}} = \frac{C_\mathrm{R} - C_\mathrm{L}}{2}\left[\frac{4}{\pi}\arctan(e^\xi) - 1\right] + \frac{C_\mathrm{R} + C_\mathrm{L}}{2}. \tag{2.23}$$

Therefore,

$$\nabla C_0^{\mathrm{OUT}}(\xi = 0) = \frac{C_\mathrm{R} - C_\mathrm{L}}{\pi\sin\eta}\boldsymbol{e}_\xi, \tag{2.24}$$

where $\boldsymbol{e}_\xi$ is a unit normal vector to constant ξ surface.

We reintroduce the length scale a and find the total diffusion flux to be

$$J_0^d = a\pi\int_\Theta^{\pi/2}\frac{C_\mathrm{R} - C_\mathrm{L}}{\pi\sin\eta}\sin\eta\cos\eta\,d\eta = a(C_\mathrm{R} - C_\mathrm{L})(1 - \sin\Theta), \tag{2.25}$$

and the total electric current is

$$J_0^e = a\frac{\phi_\mathrm{L} - \phi_\mathrm{R}}{\ln C_\mathrm{L} - \ln C_\mathrm{R}}(C_\mathrm{R} - C_\mathrm{L})(1 - \sin\Theta). \tag{2.26}$$

As mentioned earlier, the total fluxes (2.25)–(2.26) are scaled with a. When $a \to 0$, the pore shrinks and the total fluxes vanish.

The electric resistance of the channel scaled with a is

$$R = -\frac{\phi_\mathrm{L} - \phi_\mathrm{R}}{J_0^e} = \frac{\ln C_\mathrm{L} - \log C_\mathrm{R}}{a(C_\mathrm{L} - C_\mathrm{R})(1 - \sin\Theta)}. \tag{2.27}$$

The L'Hospital rule applied to (2.27) for the case $C_\mathrm{L} = C_\mathrm{R}$ implies

$$R(C_\mathrm{R} = C_\mathrm{L}) = \frac{1}{aC_\mathrm{L}(1 - \sin\Theta)}. \tag{2.28}$$

In such a case when the channel is scaled with a, the conductance of the channel is proportional to the concentration.

Finally, we would like to remark on the difference between electro-neutrality and equilibrium. Note that the solution (2.17) can be represented as

$$n_0 = p_0 = \frac{C_0^{\mathrm{OUT}}}{2} \propto e^{\phi/\alpha}, \tag{2.29}$$

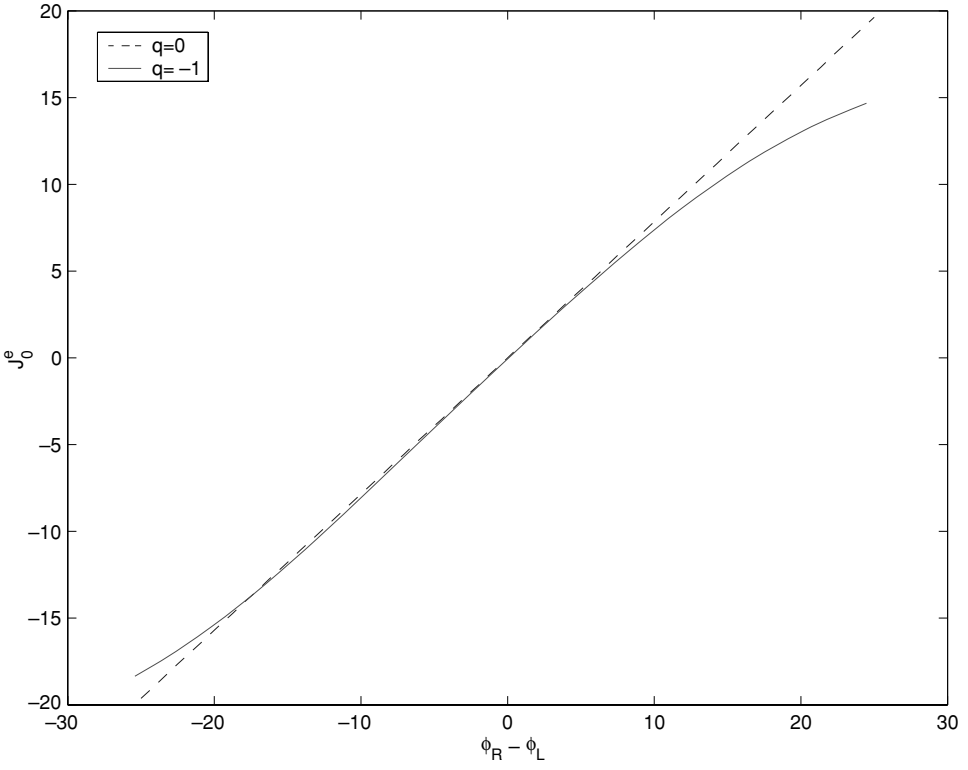

FIGURE 2. Current–voltage characteristic curve: $C_L = 3$, $C_R = 2$, (i) $q = -1$ for $-1 < z < 1$ (solid) (ii) $q \equiv 0$ (dashed). The asymptotic I–V curve is linear for the neutral channel by Ohm's law, but saturates for the charged channel. Saturation occurs at large voltages, where the asymptotic expansion is no longer valid.

which is different from the equilibrium Boltzmann distributions

$$n \propto e^{\phi}, \quad p \propto e^{-\phi}. \tag{2.30}$$

It is widely believed that away from the channel the bath may be viewed to be in equilibrium, or at least near equilibrium. Due to that belief, for example, the pair correlation function in the bath is approximated by that of equilibrium. There are good reasons supporting the equilibrium belief. First, the ion concentrations in the bath are nearly constant and the electric field almost vanishes, as in equilibrium. Second, equilibrium is characterized by zero net flux of all ions. Indeed, as we move away a distance r from the channel, the local fluxes are attenuated as $1/r^2$. Mathematically, one can view small fluxes as a perturbation to equilibrium and look for a near-equilibrium solution. The solutions (2.29) and (2.30) agree to leading order (in $1/r$), because they both tend to constant as $r \to \infty$, but their first order $1/r$ correction is different. Why is (near) equilibrium violated? The mathematical explanation is that electro-neutrality takes over the problem in the form of the small parameter ε which seems to have a profound effect more than any other physics in the problem. The physical explanation is that the total current in the baths

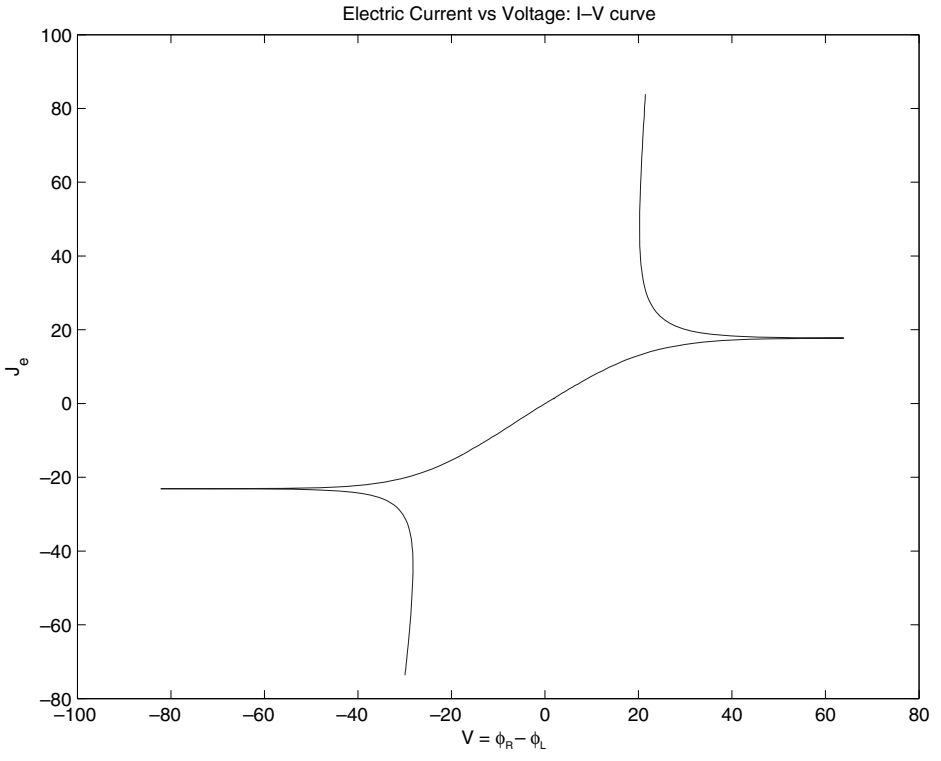

FIGURE 3. Non-physical current–voltage characteristic curve: Allowing negative concentrations gives rise to two additional branches of unbounded electric current.

must equal the current through the channel (by conservation and/or Kirchoff's law) and that is not zero.

3 One-dimensional approximation

The three-dimensional PNP system (2.1)–(2.3) is often approximated by the one-dimensional ODE system [22] (aka the slowly varying approximation)

$$\frac{\varepsilon^2}{A(z)}\frac{d}{dz}\left(A(z)\frac{d\phi}{dz}\right) = Q - q, \tag{3.1}$$

$$A(z)\left[\frac{dQ}{dz} - C\frac{d\phi}{dz}\right] = -J^e, \tag{3.2}$$

$$A(z)\left[\frac{dC}{dz} - Q\frac{d\phi}{dz}\right] = -J^d, \tag{3.3}$$

where the two transport equations are already in an integrated form and J^e, J^d are the total fluxes. The function $A(z)$ represents the surface area of equipotential and equi-concentration shells. The area function $A(z)$ grows indefinitely with z into the bath,

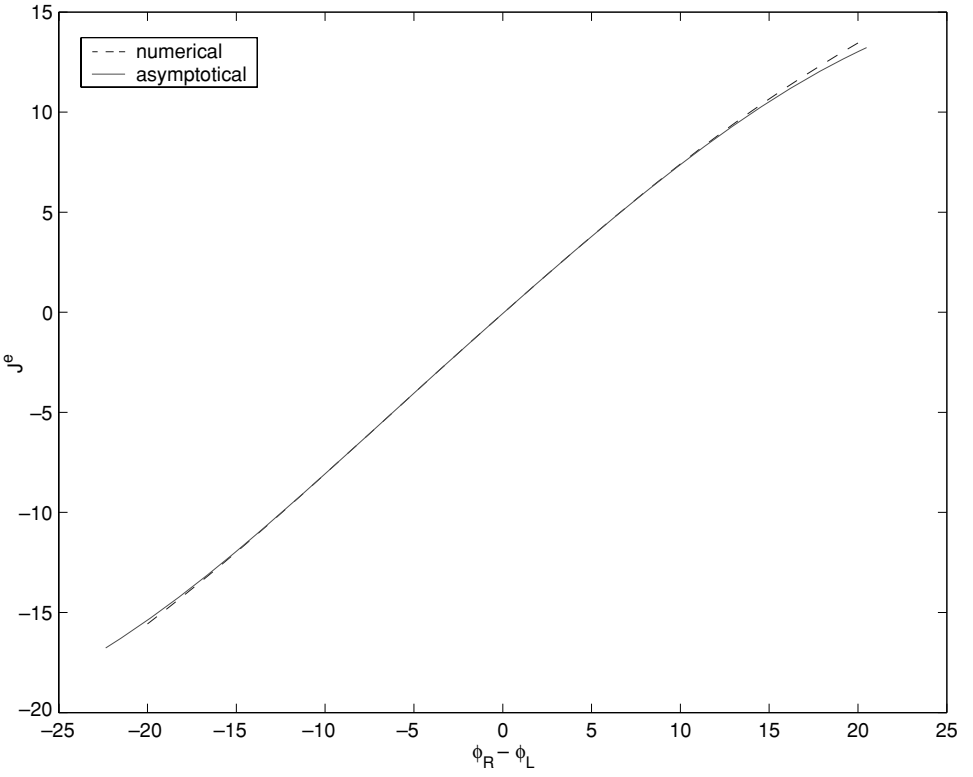

FIGURE 4. Current–voltage characteristic curve: $C_L = 3$, $C_R = 2$, $q = -1$ for $-1 < z < 1$: (i) Numerical (dashed), and (ii) Asymptotical (solid).

e.g.,

$$A(z) = 1 + z^2, \quad -\infty < z < \infty. \tag{3.4}$$

The change of variables

$$\frac{ds}{dz} = \frac{1}{A(z)} \tag{3.5}$$

maps the infinite axis $-\infty < z < \infty$ to a finite interval given $\int_{-\infty}^{\infty} \frac{dz}{A(z)} < \infty$ and the ODE system (3.1)–(3.3) to

$$\frac{\varepsilon^2}{A(z(s))^2}\frac{d^2\phi}{ds^2} = Q - q, \tag{3.6}$$

$$\frac{dQ}{ds} - C\frac{d\phi}{ds} = -J^e, \tag{3.7}$$

$$\frac{dC}{ds} - Q\frac{d\phi}{ds} = -J^d. \tag{3.8}$$

The geometry appears in merely a single place as a pre-factor in the Poisson equation. For example, for $A(z) = 1 + z^2$ (1.17) we have $s = \arctan z$, $A(z(s)) = 1 + \tan^2 s = 1/\cos^2 s$

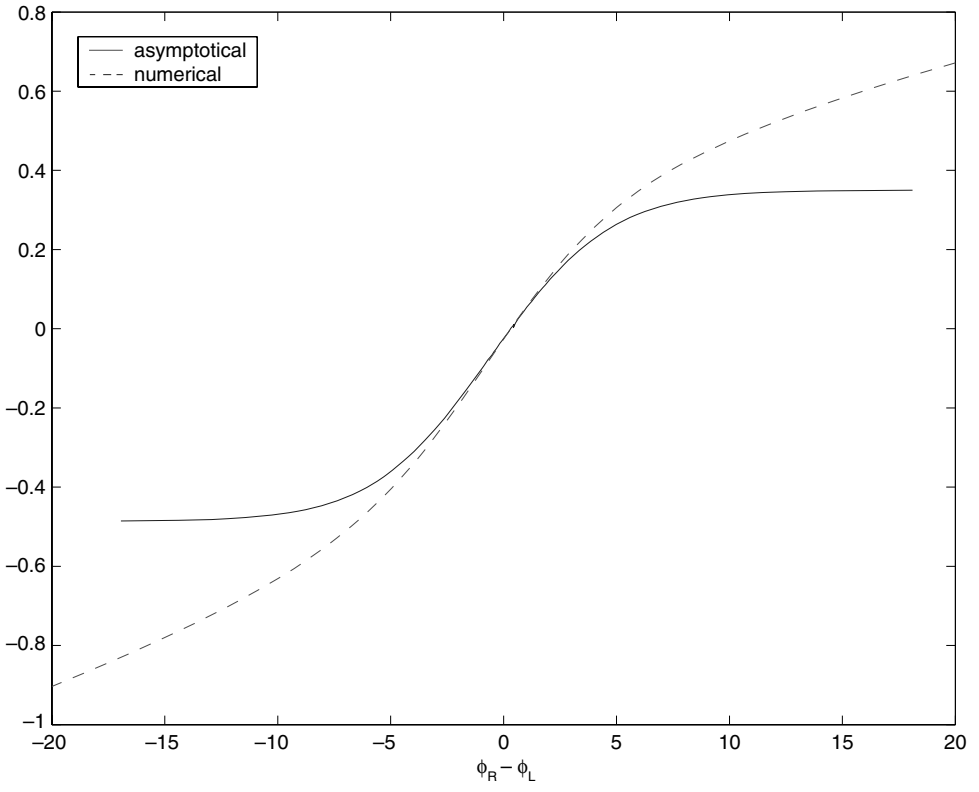

FIGURE 5. Current–voltage characteristic curve: $C_L = 0.3$, $C_R = 0.2$, $q = -1$ for $-1 < z < 1$: (i) Numerical (dashed), and (ii) Asymptotical (solid). This shows the need for a correction when V becomes large.

and the Poisson equation takes the form

$$\varepsilon^2 \cos^4 s \frac{d^2\phi}{ds^2} = Q - q, \quad -\pi/2 < s < \pi/2. \tag{3.9}$$

The transformation shows that the actual length of the interval used in [1, 16] is $L = \int_{-\infty}^{\infty} \frac{dz}{A(z)}$ rather than the physical length of the channel when modelled as a cylinder. Furthermore, the transformation also changes the location of the junctions. Note that the geometry factor is multiplied by ε^2, so it has no leading order effects, other than those mentioned above.

The ODE system (3.6)–(3.8) is a singular perturbation problem, because the small parameter ε multiplies the high-order derivative. The approximate solution consists of an outer solution and inner (boundary layer) solutions that are formed at the junctions.

The three-dimensional outer solution relations (2.7), (2.10) and (2.16) hold for the one-dimensional case as well. In particular, (2.16) reads

$$C_0^{\mathrm{OUT}} - \alpha q \ln(C_0^{\mathrm{OUT}} + \alpha q) = -J^d s + \gamma, \tag{3.10}$$

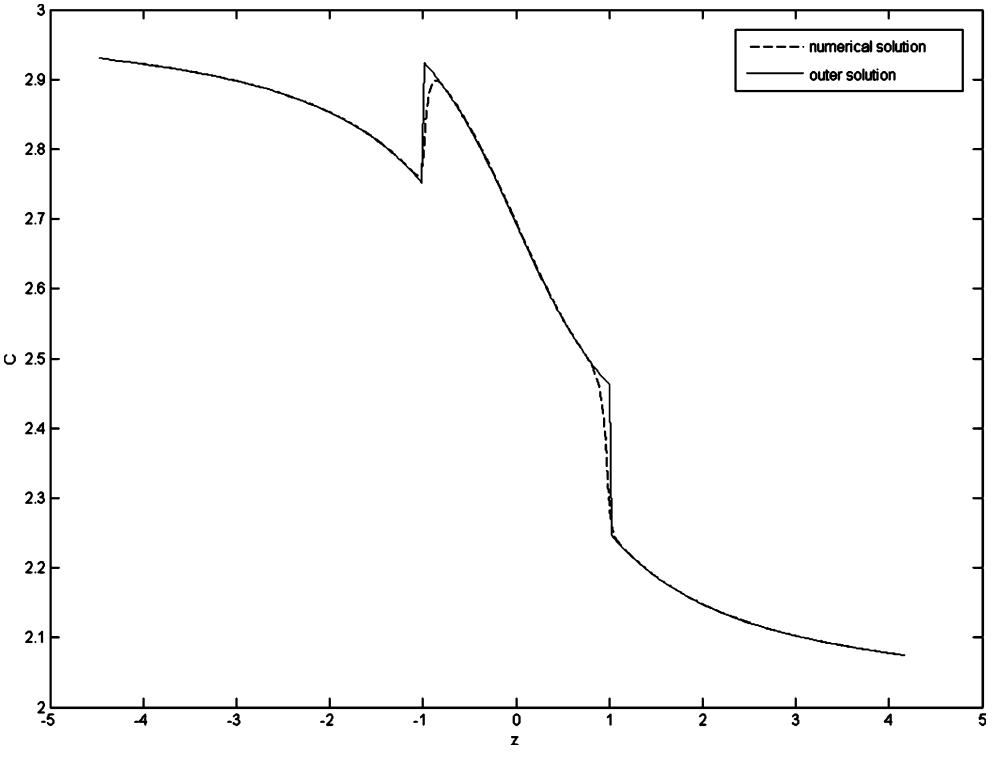

FIGURE 6. Concentration profile: numerical solution (dashed) vs. leading order outer solution (solid); $C_{\mathrm{L}} = 3$, $C_{\mathrm{R}} = 2$, $V = 0$, $\varepsilon = 0.0687$, $q = -1$ for $-1 < z < 1$.

where γ is a constant to be determined by matching (in one dimension, a harmonic function is also a linear function).

The outer solution net charge Q_0^{OUT} is discontinuous at the junction $s = s^*$, where its value jumps from 0 to q_0. For that reason, a boundary layer is introduced, characterized by the local variable $\xi = (s - s^*)/\varepsilon$. The boundary layer equations are

$$\frac{1}{A(z(s^* + \varepsilon\xi))^2}\frac{d^2\phi}{d\xi^2} = Q - q, \tag{3.11}$$

$$\frac{dQ}{d\xi} - C\frac{d\phi}{d\xi} = -\varepsilon J^e, \tag{3.12}$$

$$\frac{dC}{d\xi} - Q\frac{d\phi}{d\xi} = -\varepsilon J^d. \tag{3.13}$$

The fluxes are swept away to leading order, giving rise to the equilibrium Boltzmann distributions

$$n = \frac{1}{2}(C + Q) = \frac{1}{2}C_0 e^{\phi - \phi_0}, \tag{3.14}$$

$$p = \frac{1}{2}(C - Q) = \frac{1}{2}C_0 e^{-(\phi - \phi_0)}, \tag{3.15}$$

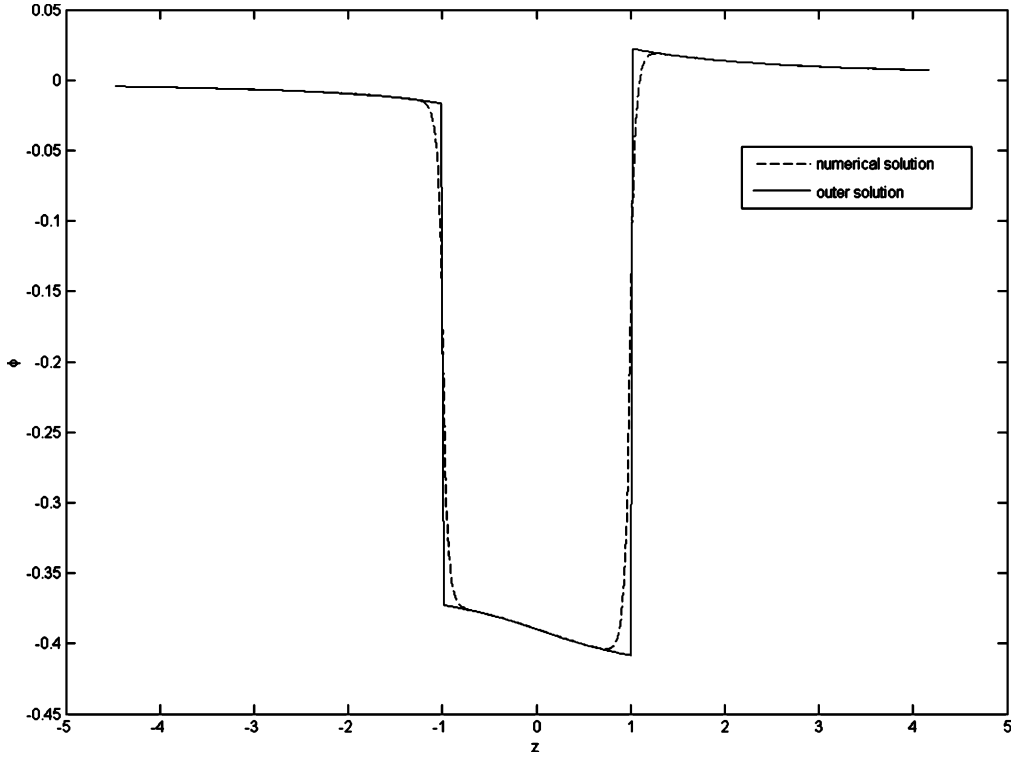

FIGURE 7. Potential profile: numerical solution (dashed) vs. leading order outer solution (solid); $C_L = 3$, $C_R = 2$, $V = 0$, $\varepsilon = 0.0687$, $q = -1$ for $-1 < z < 1$.

where C_0 and ϕ_0 are the values of the outer concentration and potential approaching the junction from the bath, where $Q_0^{OUT} = 0$. Multiplying equations (3.14) and (3.15) yields

$$np = \frac{1}{4}(C^2 - Q^2) = \frac{1}{4}C_0^2. \tag{3.16}$$

On the other side of the junction the net charge is $Q_0^{OUT} = q_0$. The charge $Q_0^{OUT} = q_0$ forms part of the capacitance measured across the membrane containing both lipid bilayers, channel protein and the pore through the protein. In general $Q_0^{OUT} = q_0$ will depend non-linearly on transmembrane voltage and will appear as a non-linear capacitance [3, 4]. Components of capacitance of this sort contribute importantly to the properties of semiconductor diodes and junctions [28]. The charge $Q_0^{OUT} = q_0$ gives the matching concentration value

$$C_q = \sqrt{C_0^2 + q_0^2} \tag{3.17}$$

(Physical concentrations are non-negative. Moreover, equation (2.10) (with $q = 0$) shows that negative concentrations lead to complex electric potential). Similarly, dividing (3.14) and (3.15) gives

$$\phi_q = \phi_0 + \frac{1}{2}\ln\left(\frac{C_q + q_0}{C_q - q_0}\right). \tag{3.18}$$

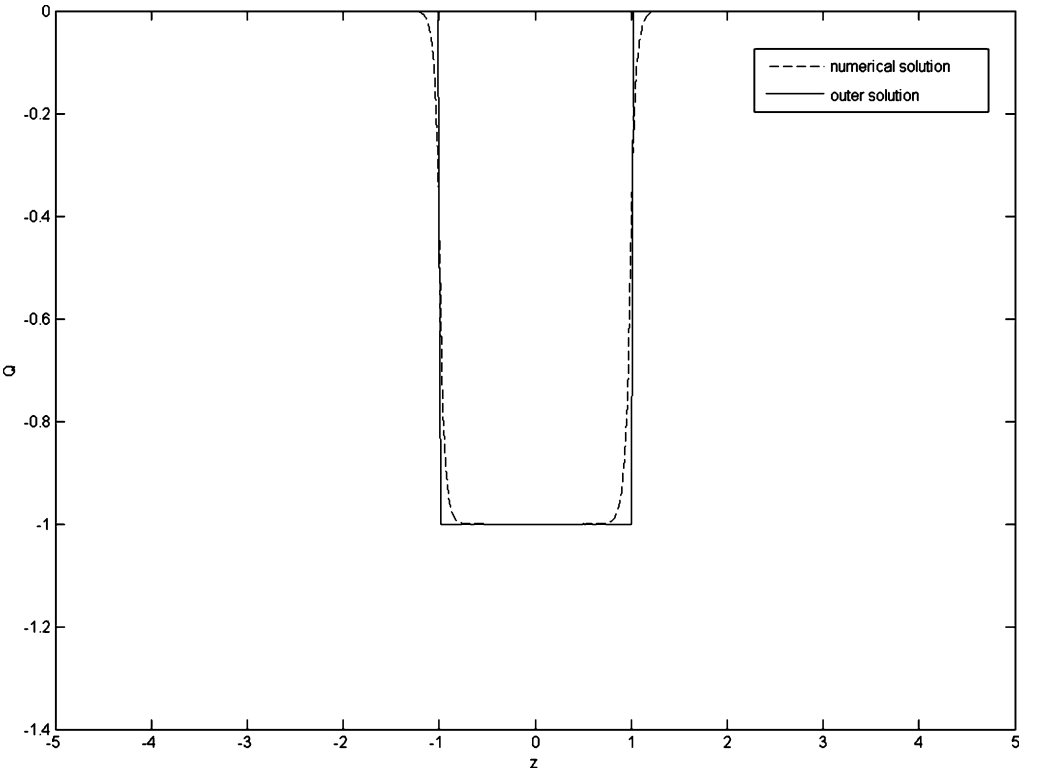

FIGURE 8. Net charge profile: numerical solution (dashed) vs. leading order outer solution (solid); $C_{\mathrm{L}} = 3$, $C_{\mathrm{R}} = 2$, $V = 0$, $\varepsilon = 0.0687$, $q = -1$ for $-1 < z < 1$.

Relations (3.17) and (3.18) match the two outer solutions across the junction, without solving explicitly the boundary layer equations (that turn out to be the Poisson–Boltzmann equations).

Gillespie [13] derived these formulas in a more general system where the fixed charge q and diffusion coefficients D_n and D_p are piecewise constant along z. On each segment i ($z^{(i)} < z < z^{(i+1)}$) where these functions are constants with values $q_0^{(i)}$, $D_n^{(i)}$ and $D_p^{(i)}$, the outer solutions (to leading order) on each segment are

$$C_0^{(i)}(z) - C_0^{(i)}\left(z^{(i)}\right) + q_0^{(i)}\frac{J_-^{(i)}}{J_+^{(i)}}\ln\left(\frac{C_0^{(i)}(z) - q_0^{(i)}\frac{J_-^{(i)}}{J_+^{(i)}}}{C_0^{(i)}\left(z^{(i)}\right) - q_0^{(i)}\frac{J_-^{(i)}}{J_+^{(i)}}}\right) + J_+^{(i)}\int_{z^{(i)}}^{z}\frac{dz'}{A(z')} = 0 \tag{3.19}$$

and

$$\phi_0^{(i)}(z) = \phi_0^{(i)}\left(z^{(i)}\right) - \frac{J_-^{(i)}}{J_+^{(i)}}\ln\left(\frac{C_0^{(i)}(z) - q_0^{(i)}\frac{J_-^{(i)}}{J_+^{(i)}}}{C_0^{(i)}\left(z^{(i)}\right) - q_0^{(i)}\frac{J_-^{(i)}}{J_+^{(i)}}}\right) \tag{3.20}$$

where

$$J_\pm^{(i)} = \frac{J^n}{D_n^{(i)}} \pm \frac{J^p}{D_p^{(i)}}. \tag{3.21}$$

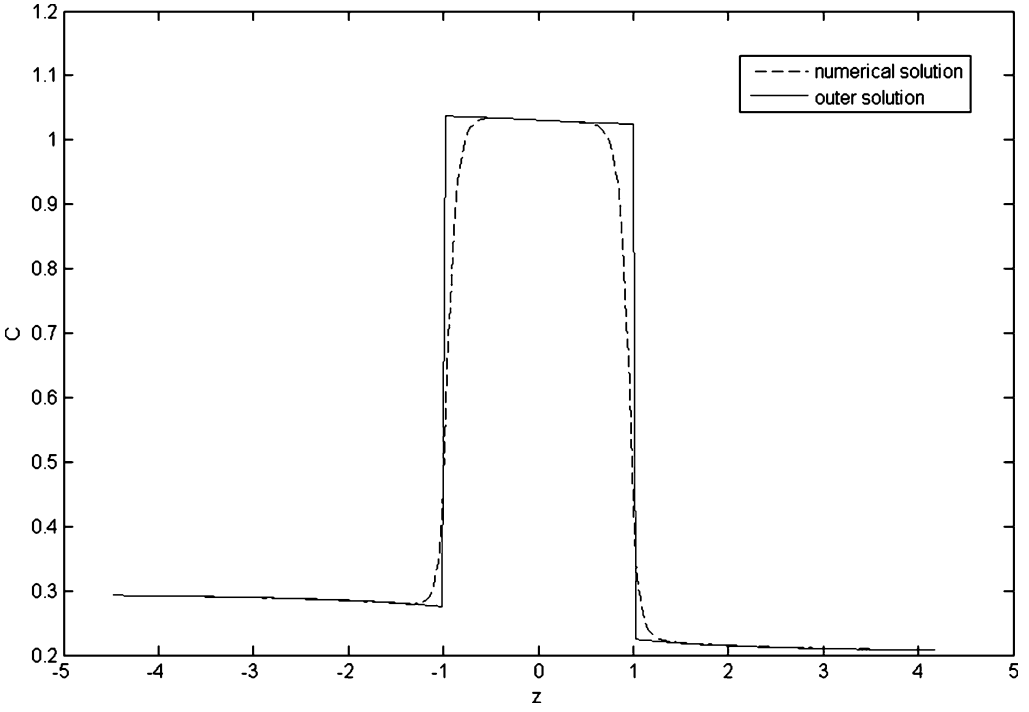

FIGURE 9. Concentration profile: numerical solution (dashed) vs. leading order outer solution (solid); $C_L = 0.3$, $C_R = 0.2$, $V = 0$, $\varepsilon = 0.0687$, $q = -1$ for $-1 < z < 1$.

To connect these outer solutions across each segment boundary (that is, to determine $C_0^{(i)}(z^{(i)})$ from $C_0^{(i-1)}(z^{(i)})$, for example),

$$C_0^{(i)}(z^{(i)}) = \sqrt{\left(C_0^{(i-1)}(z^{(i)})\right)^2 + \left(q_0^{(i)}\right)^2 - \left(q_0^{(i-1)}\right)^2} \tag{3.22}$$

and

$$\phi_0^{(i)}(z^{(i)}) = \phi_0^{(i-1)}(z^{(i)}) + \frac{1}{2}\ln\left(\frac{B^{(i)}}{B^{(i-1)}}\right) \tag{3.23}$$

where

$$B^{(i)} = \frac{C_0^{(i)}(z^{(i)}) + q_0^{(i)}}{C_0^{(i)}(z^{(i)}) - q_0^{(i)}}. \tag{3.24}$$

4 Numerical study

At this point we have all the ingredients to compute the current. In the case of three segments (two baths and the charged channel), one can determine the current with the following algorithm. Given a diffusion current J_0^d the concentration C_0 at the entry to the junction is calculated using (3.10) (with $q = 0$). The matching condition (3.17) then

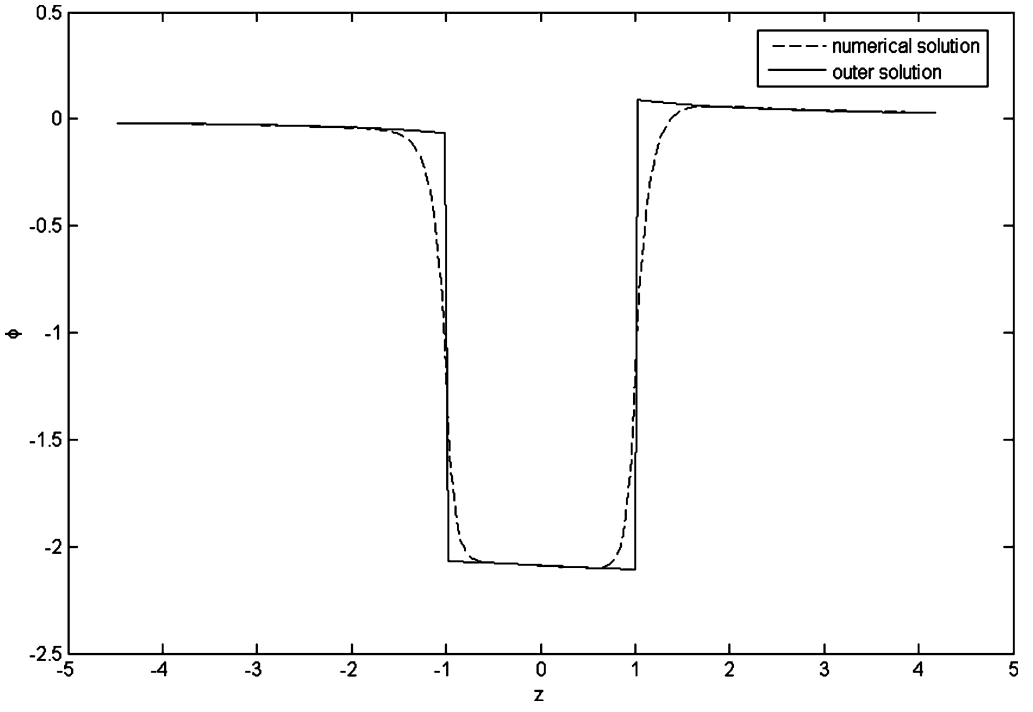

FIGURE 10. Potential profile: numerical solution (dashed) vs. leading order outer solution (solid); $C_L = 0.3$, $C_R = 0.2$, $V = 0$, $\varepsilon = 0.0687$, $q = -1$ for $-1 < z < 1$.

gives the concentration at the other side of the junction, into the charged zone at both ends. Equation (3.10) is used once again, this time with $q = q_0$, and uniquely determines the value of α, which by equation (2.14) is the ratio of the electric and diffusion currents. The electric flux is then used to calculate the potential outside the junction in the left bath (2.10) and using (3.18) into the charged zone and once again in the right bath, resulting in the value of ϕ_R. Overall, we find the potential $V = \phi_R - \phi_L$ and electric currents J_0^e as functions of the diffusion current J_0^d. The curve (V, J_0^e) is known as the I–V (current–voltage) characteristic curve of the device.

Figure 2 shows asymptotical current–voltage curves corresponding to bath concentrations $C_L = 3$ and $C_R = 2$ and two different permanent charge profiles: (i) $q = -1$ for $-1 < z < 1$ with $A(z) = 1 + z^2$ (or $q = -1$ for $|s| < \pi/4$ and $q = 0$ for $\pi/4 < |s| < \pi/2$), and (ii) $q \equiv 0$ (no permanent charge), where Ohm's law predicts linear I–V curve.

For the negative charged channel, the values of J_0^d do not exceed $\frac{4}{\pi}C_L$ and $-\frac{4}{\pi}C_R$, because non-physical negative concentrations are excluded. In such a case there is a single electric current for a given applied potential. If one allows non-physical negative concentrations and complex electric potential values, then 'mathematical' multiple currents may be found [11], as shown in Figure 3 for sufficiently high voltages.

Next, we compare the leading order asymptotical result with the numerical I–V curve, obtained by solving the ODE system (3.1)–(3.3) numerically with $\varepsilon = 0.0687$. Figure 4

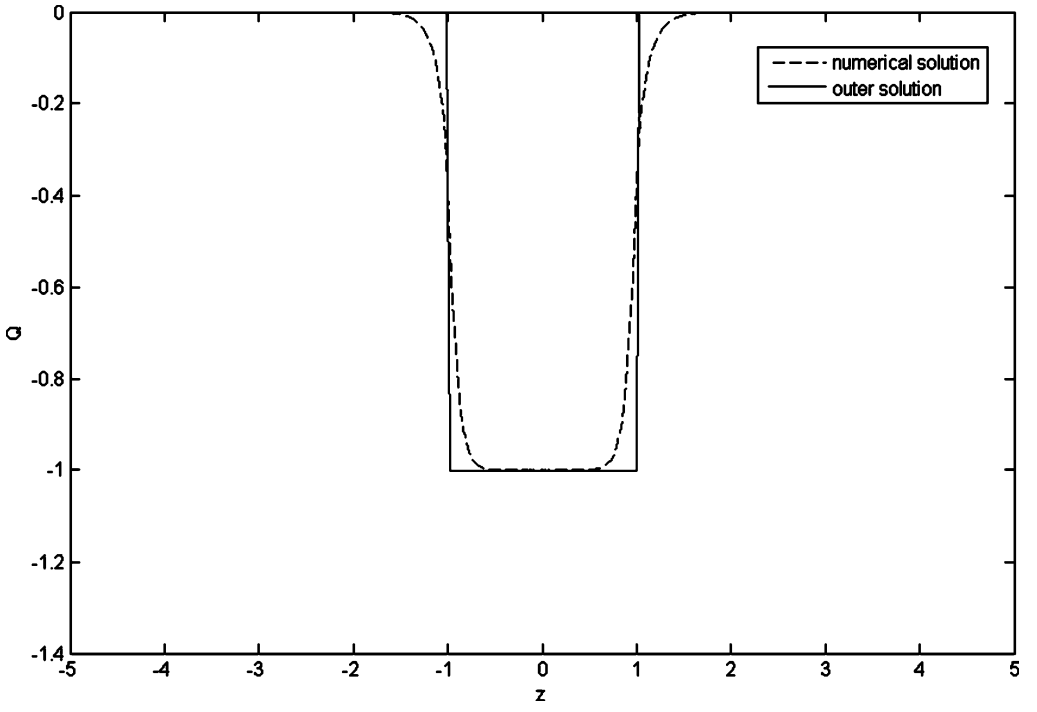

FIGURE 11. Net charge profile: numerical solution (dashed) vs. leading order outer solution (solid); $C_L = 0.3$, $C_R = 0.2$, $V = 0$, $\varepsilon = 0.0687$, $q = -1$ for $-1 < z < 1$.

shows an excellent agreement between the numerical and asymptotical results for concentration boundary values $C_L = 3$ and $C_R = 2$. The approximation gets poorer at very high voltages, where we enter a different asymptotical regime, as V is no longer $O(1)$ but rather $O(1/\varepsilon)$, violating our perturbation analysis assumptions. In particular, even though the asymptotical electric current saturates to a limit value as $V \to \pm\infty$, the numerical electric current grows up indefinitely. This behaviour is better depicted in Figure 5 that shows the I–V curve for $C_L = 0.3$ and $C_R = 0.2$.

Finally, we compare the numerical profiles of concentration, net charge and potential with those predicted by the leading order outer expansion. Figures 6–8 show this comparison for the negative charged channel with $C_L = 3$, $C_R = 2$, $V = 0$ and $\varepsilon = 0.0687$. The figures demonstrate that the outer solution is a very good approximation of the numerical solution, but for the two boundary layers where the permanent charge is discontinuous, as predicted by the above analysis. Figures 9–11 show the successful approximation when the boundary concentration values are changed to $C_L = 0.3$ and $C_R = 0.2$. The total electric current, which is the single measured output of the device, is constant and therefore can be evaluated at a single point away from the boundary layers, where the outer and numerical solutions show an excellent agreement. In that sense, the exact boundary layer profiles are unimportant for the determination of the fluxes.

Our work shows the importance of the access regions to channel conduction. It is clear that analyses without the access region can be misleading. We expect that different types

of channels will have access regions specialized for their particular evolved function. Few complete structures of channels—including access regions—are known today to evaluate this idea.

5 Acknowledgements

The work was supported in part by NIH Grant GM076013 to Robert Eisenberg. We wish to thank Chris Breward for organizing the Maths in Medicine Study Group held at Oxford University in September 2005, from which the report [6] was written. We would also like to thank the other participants of the study group, in particular, Jon Chapman, Peter Howell, John King, Colin Please, Giles Richardson and Tom Witelski for helpful and fun discussions.

References

[1] Barcilon, V., Chen, D.-P., Eisenberg, R. S. & Jerome, J. W. (1997) Qualitative properties of steady-state Poisson–Nernst–Planck systems: Perturbation and simulation study. *SIAM J. Appl. Math.* **57**(3), 631–648.

[2] Barthel, J., Krienke, H. & Kunz, W. (1998) *Physical Chemistry of Electrolyte Solutions: Modern Aspects*, Springer, New York.

[3] Bezanilla, F. & Armstrong, C. M. (1974) Gating currents of the sodium channels: Three ways to block them. *Science*. **183**, 753–754.

[4] Bezanilla, F. & Stefani, E. (1994) Voltage-dependent gating of ionic channels. *Annu. Rev. Biophys. Biomol. Struct*. **23**, 819–846.

[5] Blum, L., Vericat, F. & Fawcett, W. R. (1992) On the mean spherical approximation for hard ions and dipoles. *J. Chem. Phys.* **96**, 3039.

[6] Chapman, J., Norbury, J., Please, C. & Richardson, G. Ions in solutions and protein channels. In: *Fifth Mathematics in Medicine Study Group*, University of Oxford, September 2005, available online: http://www.maths.ox.ac.uk/ociam/Study-Groups/MMSG05/reports/ionreport.pdf

[7] Chhih, A., Bernard, O., Barthel, J. M. G. & Blum, L. (1994) Transport coefficients and apparent charges of concentrated electrolyte solutions: Equations for practical use. *Ber. Bunsenges. Phys. Chem.* **98**, 1516–1525.

[8] Durand-Vidal, S., Simonin, J.-P. & Turq, P. (2000) *Electrolytes at Interfaces*, Boston, Kluwer.

[9] Durand-Vidal, S., Turq, P., Bernard, O., Treiner, C. & Blum, L. (1996) New perspectives in transport phenomena in electrolytes. *Phys. A* **231**, 123–143.

[10] Eisenberg, R. S. (1998) Ionic channels in biological membranes: Electrostatic analysis of a natural nano-tube. *Contemp. Phys.* **39**, 447–466.

[11] Eisenberg, R. S. & Liu, W. (2007) Poisson–Nernst–Planck systems for ion channels with permanent charges. *SIAM J. Math. Anal.* **38**, 1932–1966.

[12] Fawcett, W. R. (2004) *Liquids, Solutions, and Interfaces: From Classical Macroscopic Descriptions to Modern Microscopic Details*, Oxford University, New York.

[13] Gillespie, D. (1999) *A Singular Perturbation Analysis of the Poisson–Nernst–Planck System: Applications to Ionic Channels*. PhD dissertation, Rush University, Chicago.

[14] Gillespie, D., Xu, L., Wang, Y. & Meissner, G. (2005) (De)constructing the ryanodine receptor: Modeling ion permeation and selectivity of the calcium release channel. *J. Phys. Chem. B* **109**, 15598–15610.

[15] Hille, B. (2001) *Ionic Channels of Excitable Membranes*, 3rd ed., Sinauer Associates, Sunderland, MA, pp. 1–814.

[16] Liu, W. (2005) Geometric singular perturbation approach to steady-state Poisson–Nernst–Planck systems. *SIAM J. Appl. Math.* **65**, 754–766.
[17] Markowich, P. A. (1984) A singular perturbation analysis of the fundamental semiconductor device equations. *SIAM J. Appl. Math.* **44**(5), 896–928.
[18] Markowich, P. A. (1986) *The Stationary Semiconductor Device Equations*, Springer-Verlag, New York.
[19] Markowich, P. A. & Ringhofer, C. A. (1984) A singularly perturbed boundary value problem modelling a semiconductor device. *SIAM J. Appl. Math.* **44**(2), 231–256.
[20] Markowich, P. A., Ringhofer, C. A. & Schmeiser, C. (1990) *Semiconductor Equations*, Springer-Verlag, New York.
[21] Nonner, W., Catacuzzeno, L. & Eisenberg, R. S. (2000) Binding and selectivity in L-type calcium channels: A mean spherical approximation. *Biophys. J.* **79**, 1976–1992.
[22] Nonner, W. & Eisenberg, R. S. (1998) Ion permeation and glutamate residues linked by Poisson–Nernst–Planck theory in L-type calcium channels. *Biophys. J.* **75**(3), 1287–1305.
[23] Schuss, Z., Nadler, B. & Eisenberg, R. S. (2001) Derivation of PNP equations in bath and channel from a molecular model. *Phys. Rev. E* **64**(2–3), 036116.
[24] Simonin, J.-P., Blum, L. & Turq, P. (1996) Real ionic solutions in the mean spherical approximation. 1. Simple salts in the primitive model. *J. of Phys. Chem.* **100**, 7704–7709.
[25] Siwy, Z., Powell, M. R., Kalman, E., Astumian, R. D. & Eisenberg, R. S. (2006) Negative incremental resistance induced by calcium in asymmetric nanopores. *Nano Lett.* **6**, 473–477.
[26] Siwy, Z., Powell, M. R., Kalman, E., Trautmann, C. & Eisenberg, R. S. (2006) Calcium-induced voltage gating in single conical nanopores. *Nano Lett.* **6**, 1729–1734.
[27] Smith, G. R. & Sansom, M. S. P. (1998) Dynamic properties of Na+ ions in models of ion channels: A molecular dynamics study. *Biophys. J.* **75**, 2767–2782.
[28] Sze, S. M. (1981) *Physics of Semiconductor Devices*, John Wiley & Sons, New York.
[29] Tieleman, D. P. & Berendsen, H. J. C. (1998) A molecular dynamics study of the pores formed by *Escherichia coli* OmpF Porin in a fully hydrated palmitoyloleoylphosphatidylcholine bilayer. *Biophys. J.* **74**, 2786–2801.